AGU PUBLICATIONS

JGR

Journal of Geophysical Research: Atmospheres

RESEARCH ARTICLE
10.1002/2015JD024566

This article is a companion to *Wang et al.* [2016] doi:10.1002/2015JD024556.

**Key Points:**
- Large (up to 12 ppbv $N_2O_5$) but infrequent nocturnal NOx outflow from the Pearl River Delta
- Average $N_2O_5$ uptake coefficients $0.014 \pm 0.007$, in line with residual layer measurements in the U.S.
- Daytime $N_2O_5$ follows predicted steady state but rapidly produces soluble nitrate in fog

**Correspondence to:**
S. S. Brown,
steven.s.brown@noaa.gov

**Citation:**
Brown, S. S., et al. (2016), Nighttime chemistry at a high altitude site above Hong Kong, *J. Geophys. Res. Atmos.*, *121*, 2457–2475, doi:10.1002/2015JD024566.

Received 24 NOV 2015
Accepted 5 FEB 2016
Accepted article online 11 FEB 2016
Published online 11 MAR 2016



# Nighttime chemistry at a high altitude site above Hong Kong

**Steven S. Brown[1,2], William P. Dubé[1,3], Yee Jun Tham[4], Qiaozhi Zha[4], Likun Xue[4], Steven Poon[4], Zhe Wang[4], Donald R. Blake[5], Wilson Tsui[6], David D. Parrish[1,3], and Tao Wang[4]**

[1]Chemical Sciences Division, NOAA Earth System Research Laboratory, Boulder, Colorado, USA, [2]Department of Chemistry and Biochemistry, University of Colorado Boulder, Boulder, Colorado, USA, [3]Cooperative Institute for Research in Environmental Sciences, University of Colorado Boulder, Boulder, Colorado, USA, [4]Department of Civil and Environmental Engineering, Hong Kong Polytechnic University, Hong Kong, China, [5]Department of Chemistry, University of California, Irvine, California, USA, [6]PTC International Limited, Hong Kong, China

**Abstract** Nighttime reactions of nitrogen oxides influence ozone, volatile organic compounds, and aerosol and are thus important to the understanding of regional air quality. Despite large emissions and rapid recent growth of nitrogen oxide concentrations, there are few studies of nighttime chemistry in China. Here we present measurements of nighttime nitrogen oxides, $NO_3$ and $N_2O_5$, from a coastal mountaintop site in Hong Kong adjacent to the megacities of the Pearl River Delta region. This is the first study of nighttime chemistry from a site within the residual layer in China. Key findings include the following. First, highly concentrated urban $NO_x$ outflow from the Pearl River Delta region was sampled infrequently at night, with $N_2O_5$ mixing ratios up to 8 ppbv (1 min average) or 12 ppbv (1 s average) in nighttime aged air masses. Second, the average $N_2O_5$ uptake coefficient was determined from a best fit to the available steady state lifetime data as $\gamma(N_2O_5) = 0.014 \pm 0.007$. Although this determination is uncertain due to the difficulty of separating $N_2O_5$ losses from those of $NO_3$, this value is in the range of previous residual layer determinations of $N_2O_5$ uptake coefficients in polluted air in North America. Third, there was a significant contribution of biogenic hydrocarbons to $NO_3$ loss inferred from canister samples taken during daytime. Finally, daytime $N_2O_5$ mixing ratios were in accord with their predicted photochemical steady state. Heterogeneous uptake of $N_2O_5$ in fog is determined to be an important production mechanism for soluble nitrate, even during daytime.

## 1. Introduction

The emissions and atmospheric chemistry of nitrogen oxides ($NO_x = NO + NO_2$) influence air quality and climate through their regulation of secondary pollutants such as ozone and aerosols. Nitrogen oxides undergo both photochemical (sunlight driven) and dark (requiring the absence of sunlight) chemical cycles. During daytime, they act as catalysts in the well-known mechanism for the production of tropospheric ozone. At night, they participate in a separate set of reactions that removes both ozone and nitrogen oxides from the atmosphere, initiates the oxidation of volatile organic compounds, serves as a source of secondary aerosol, and activates halogen species [*Brown and Stutz*, 2012]. The oxidation of $NO_2$ by $O_3$, which produces the nitrate radical, $NO_3$, initiates these chemical cycles.

$$NO_2 + O_3 \rightarrow NO_3 + O_2 \quad (1)$$

$$NO_3 + NO_2 \leftrightarrows N_2O_5 \quad (2)$$

$$NO_3 + VOC \rightarrow Products \quad (3)$$

$$N_2O_5 + H_2O(het) \rightarrow 2HNO_3 \quad (4)$$

$$N_2O_5 + Cl^-(het) \rightarrow ClNO_2 + NO_3^- \quad (5)$$

The nitrate radical is short lived during daytime due to its rapid photolysis and reaction with NO, both of which serve to regenerate $NO_x$ and effectively reverse reaction (1). The $NO_3$ concentration increases during nighttime, together with that of dinitrogen pentoxide, $N_2O_5$, with which it is in thermal equilibrium via reaction (2). The nitrate radical is a strong oxidant of unsaturated hydrocarbons and reduced sulfur compounds. It is therefore highly reactive with biogenic hydrocarbons such as isoprene and monoterpenes in terrestrial environments [*Winer et al.*, 1984] and dimethyl sulfide in marine environments [*Platt et al.*, 1990]. Nighttime reactions of $NO_3$ with isoprene and monoterpenes may be an important mechanism for

production of secondary organic aerosol [*Pye et al*., 2010]. Dinitrogen pentoxide reacts via heterogeneous uptake to aerosol to yield soluble nitrate ($HNO_3$ or $NO_3^-$) or nitryl chloride, $ClNO_2$. The latter undergoes morning photolysis subsequent to its nighttime production and acts as a source of atomic chlorine radicals and $NO_2$. This mechanism recycles $NO_2$ that would otherwise be converted to soluble nitrate if all $N_2O_5$ uptake proceeded through reaction (4). The availability of aerosol phase chloride determines the competition between reactions (4) and (5) [*Bertram and Thornton*, 2009; *Roberts et al*., 2009]. Recent field studies have shown that $ClNO_2$ production is widespread and represents a large source of reactive halogens to the troposphere [*Thornton et al*., 2010].

Production of $NO_3$ via reaction (1) depends linearly on the mixing ratios of both $O_3$ and $NO_2$. Emissions of nitrogen oxides have been declining steadily in North America and Europe but increasing rapidly in Asia [*Hilboll et al*., 2013; *Russell et al*., 2012]. The recent trend in satellite-derived $NO_2$ column over large cities in China shows an increase of +5–10% $yr^{-1}$ [*Hilboll et al*., 2013]. Surface ozone concentrations have been declining across broad areas of the United States in response to declining $NO_x$ emissions [*Cooper et al*., 2012; *Simon et al*., 2014]. Reported $O_3$ data in China are not as extensive as those in the U.S. and Europe, but reports of surface ozone in China suggest large ozone production downwind of Beijing [*Wang et al*., 2006] but only modest trends within the city itself [*Tang et al*., 2009]. In southern China, there is a positive trend (0.6–0.9 ppbv $yr^{-1}$) in surface ozone during the winter season at a coastal site in Hong Kong associated with outflow from mainland China during that season [*Wang et al*., 2009]. These trends in $NO_2$ and $O_3$ suggest generally decreasing rates of $NO_3$ and $N_2O_5$ production in North America and Europe but a rapidly increasing rate of nighttime chemical reactions in China, with the potential to drive the associated chemical cycles.

Despite its importance to regional air quality and despite the likely rapid increase in the rate of nighttime chemistry, investigations of nighttime nitrogen oxides in China remain relatively sparse. Several studies have identified the role of $N_2O_5$ uptake in production of aerosol nitrate, a significant component of secondary inorganic aerosol. *Pathak et al*. [2009, 2011] found that heterogeneous $N_2O_5$ uptake led to accumulation of fine aerosol nitrate downwind of Beijing and Shanghai megacities even under conditions of high aerosol acidity. Recent studies of aerosol loading and composition across China have identified nitrate as an important component (7–14% on average) and have noted the contribution of multiphase chemistry initiated by $NO_3$ [*Guo et al*., 2014; *Huang et al*., 2014]. A model study of a severe winter haze episode in Beijing showed that inclusion of heterogeneous nitrogen oxide reactions was essential to reproduce observations [*Zheng et al*., 2015]. Similarly, analysis of a winter haze event in Hong Kong with high nitrate loadings showed that $N_2O_5$ uptake contributed significantly to the nitrate aerosol accumulation rate even during daytime [*Xue et al*., 2014]. Although $N_2O_5$ production and uptake is a major process underlying aerosol pollution in China, these field studies lack direct measurements of this key intermediate. *Wang et al*. [2013] presented measurements of $NO_3$ by differential optical absorption spectroscopy, together with $NO_2$ and $N_2O_5$ calculated via the equilibrium in reaction (2), within the urban area of Shanghai during August–October 2011. These surface level measurements found $NO_3$ production rates via reaction (1) of several parts per billion per hour and evidence that sinks for $NO_3$ and $N_2O_5$ were dominated by heterogeneous reactions of the latter.

Nighttime reactions of nitrogen oxides are often difficult to characterize in field studies due to the lack of mixing within the planetary boundary layer at night [*Stutz et al*., 2004]. Surface level measurements are representative of either a nocturnal boundary layer, with a depth on the order of 100 m, or a surface layer that may be only tens of meters deep [*Stull*, 1988]. Measurements at the surface do not characterize the composition or chemistry of the much deeper residual layer, where the largest mass from the previous day's emission resides. Strategies for probing the residual layer include measurements from aircraft [*Brown et al*., 2007; *Kennedy et al*., 2011], tall towers [*Benton et al*., 2010; *Wagner et al*., 2013], or terrain features that lie within the residual layer [*Crowley et al*., 2010].

Here we present measurements of nighttime nitrogen oxides and related species from Tai Mo Shan, a coastal mountaintop site in Hong Kong, China, with an elevation of 957 m. Measurements took place during November and December 2013, during the latter part of the season with high ozone pollution in Hong Kong [*Wang et al*., 2009]. The Tai Mo Shan campaign included measurements of $NO_3$, $N_2O_5$, $ClNO_2$, HONO, $O_3$, VOCs, particle size distributions, and aerosol ionic composition. The study provides a comprehensive

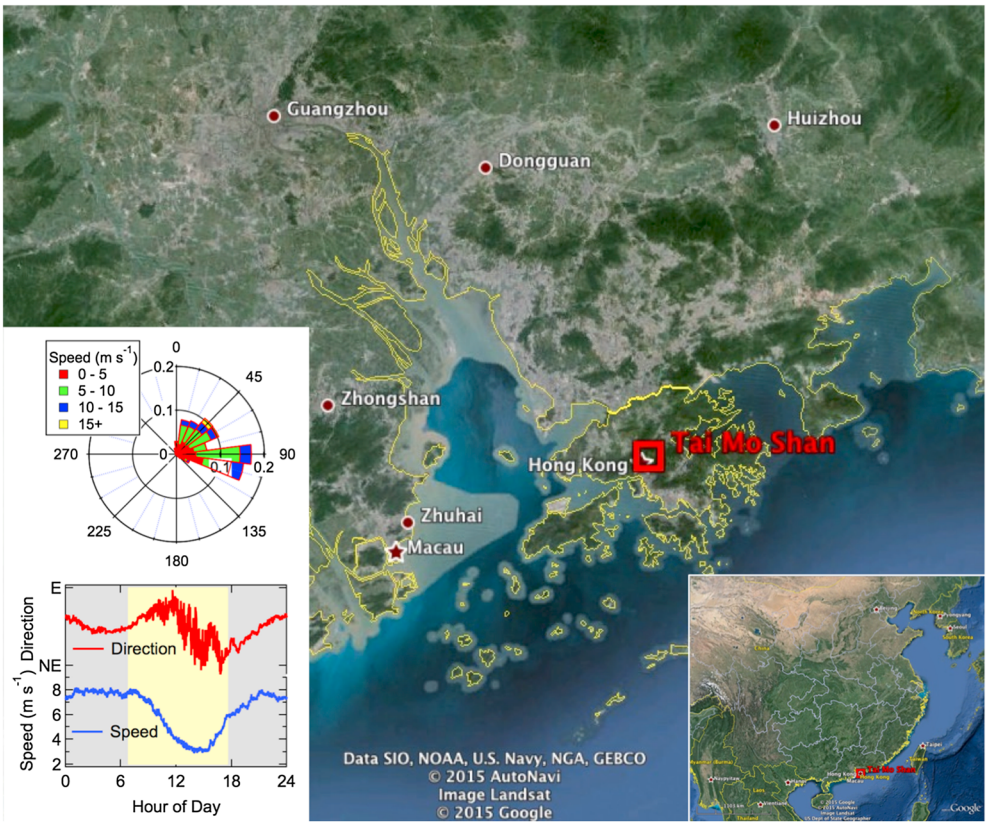


**Figure 1.** Map of the Pearl River Delta area of southeast China showing the location of the Tai Mo Shan mountaintop observatory. The left inset shows a wind rose (top) and the diurnal average wind direction and wind speed during the study period (bottom). Winds were exclusively from the east and northeast and most commonly between 5 and 10 m $s^{-1}$. Nighttime and early morning winds were strong, while late afternoon winds were slack. The average direction rotated slightly to the northeast in the afternoon during the period of slower average wind speed.

analysis of nighttime chemistry in an Asian megacity and the first observations of nighttime chemistry within the residual layer in Asia. This paper examines the nighttime chemistry of $NO_3$ and $N_2O_5$, while a companion paper [*Wang et al.*, 2016] describes observations and analysis of nitryl chloride, $ClNO_2$.

## 2. Field Site and Instruments

The Tai Mo Shan observatory is located north of major population centers of Hong Kong (Kowloon and Hong Kong) and to the south of Shenzhen in mainland China (Figure 1). It is the highest point in Hong Kong at 957 m. This altitude is near the top of the average daytime mixed layer height in Hong Kong during autumn (1.2 km) and winter (1.0 km)[*Yang et al.*, 2013]. Thus, during the November–December study period, the site would lie near the top of the residual layer at night, with the potential to sample from the free troposphere at times. Although the site was high enough to encounter clouds and was thus frequently impacted by fog during the study period (see below), measured levels of pollutants were nearly always characteristic of at least a moderately polluted boundary layer. Median (average) total reactive nitrogen, $NO_y$, was 6.15 ppbv (7.88 ppbv), with an interquartile range (25th–75th percentiles) of 4.51–9.13 ppbv and a 10th–90th percentile range of 3.14–13.98 ppbv. Thus, regardless of whether the sampled air was influenced more by the boundary layer or free troposphere, it was always impacted by regional pollution. All instruments were housed in a small, custom-built shelter with inlets affixed to a scaffold above the shelter roof at a height of 6 m above ground level at the mountaintop site.

A companion paper on $ClNO_2$ observations during this campaign [*Wang et al.*, 2016] gives a detailed description of the instrumentation for trace gas, aerosol, radiation, and meteorological measurements. The focus of the current paper is on the analysis of $NO_3$ and $N_2O_5$. Briefly, these species were measured using diode laser

cavity ring-down spectroscopy (CRDS) at 662 nm [*Wagner et al*., 2011]. The instrument measures $NO_3$ directly by optical extinction on its strong, 662 nm absorption band. It measures the sum of $NO_3$ and $N_2O_5$ simultaneously in a separate channel through a heated inlet that thermally dissociates $N_2O_5$ to $NO_3$. Precision and accuracy for $N_2O_5$ are $\leq$3 parts per thousand by volume (pptv) ($2\sigma$, 1 s) [*Wagner et al*., 2011] and ±12% [*Fuchs et al*., 2008], respectively. The stated precision and accuracy for $NO_3$ is normally approximately equivalent to that of $N_2O_5$. However, for the data from this campaign, $NO_3$ was observed to be substantially lower (60%) than the mixing ratio predicted by the $NO_3$-$N_2O_5$ equilibrium in reaction (2), contrary to experience with previous airborne and ground-based measurements with this technique [*Brown et al*., 2003b; *Osthoff et al*., 2007], indicating a large loss for this species in the instrument inlet during this campaign. The reported $NO_3$ was corrected for this loss factor based on its predicted ratio to $N_2O_5$. Because of the much larger associated uncertainty in $NO_3$ for this campaign, and because the resulting $NO_3$ measurement is not independent of $N_2O_5$, the analysis reported in this paper relies on the $N_2O_5$ measurement only. The inlet was constructed of 6 m of 1/4 inch (6.35 mm) OD, 5/32 inch (4.0 mm) ID fluorinated ethylene propylene Teflon tubing, with a restriction at the end of the inlet that dropped the pressure below 300 mbar. The total volumetric flow in the inlet was approximately 20 L/min, for a residence time of 0.2 s. It is not clear whether the $NO_3$ loss occurred in this inlet, the filter housing (residence time 0.06 s), or the tubing used to construct the sample cells around the optical detection axis (residence time 0.25 s). Periodic exchanges of the external inlet tubing did not change the apparent $NO_3$ transmission. Transmission of $N_2O_5$ is generally much greater than that of $NO_3$ [*Fuchs et al*., 2008], and comparison between the CRDS $N_2O_5$ and a measurement based on chemical ionization mass spectrometry showed excellent agreement [*Wang et al*., 2016]. Thus, the $N_2O_5$ measurement is taken here as correct, while the $NO_3$ measurement is assumed to suffer from inlet losses during this campaign. Transmission of $N_2O_5$ has been found independent of relative humidity (RH) up to 95% [*Fuchs et al*., 2008]. However, potential inlet $N_2O_5$ loss at 100% RH (i.e., fog) is unknown. Section 5 discusses $N_2O_5$ measurement in polluted, daytime fog, where small but nonzero $N_2O_5$ was observed and taken to be accurate.

The same instrument also measures NO, $NO_2$, $NO_y$, and $O_3$ by diode laser CRDS at 405 nm. In this case, $NO_2$ is measured directly by optical extinction, and NO, $O_3$, and $NO_y$ are converted quantitatively to $NO_2$ in three additional, separate measurement channels. Measurement precision is equal to or better than 60 pptv ($2\sigma$, 1 s), and the accuracy is 3% for $NO_2$ and $O_3$, 5% for NO, and 12% for $NO_y$. Linear fits using orthogonal distance regressions of $NO_2$, NO, and $NO_y$ measured by CRDS against measurements from a chemiluminescence analyzer showed slopes of $0.97 \pm 0.01$, $0.91 \pm 0.01$, and $1.11 \pm 0.01$, respectively (errors are $2\sigma$ fit errors). Comparison of CRDS $O_3$ to a commercial 254 nm UV absorption instrument showed a slope of 1.00. The CRDS measurements operated from 15 November to 6 December 2013, while the chemiluminescence $NO_x$, $NO_y$, and UV absorption $O_3$ operated through 14 December. Data analyzed in this manuscript use CRDS $NO_2$, $NO_y$, and $O_3$ but use the other instruments to fill in data gaps in the CRDS instrument, including the entire period after 6 December.

As described in the companion paper [*Wang et al*., 2016], $ClNO_2$ was measured by iodide ion chemical ionization mass spectrometry with a precision of 4 pptv ($2\sigma$, 1 min) and an accuracy of 20%.

## 3. Measurement Overview

The local airflow at Tai Mo Shan was exclusively from the east and northeast as the wind rose in Figure 1 shows. This direction was mainly onshore from the South China Sea and occasionally parallel to the coastline or slightly offshore from mainland China. During the night and early morning, winds were consistently stronger and more easterly (onshore), with an average wind speed of 8 m $s^{-1}$. During late morning through late afternoon the average wind speed gradually slackened to 3 m $s^{-1}$ by 15:00. A slight rotation of the average wind direction toward the northeast, and slightly more from mainland China, accompanied the afternoon wind slackening. Most individual days had slower afternoon wind speeds, but fewer days exhibited the local wind direction shift. Despite a local wind direction from the South China Sea, air masses were never observed to be free of pollution, indicating the importance of mixing between continental outflow and the prevailing easterly flow, as described in more detail in the companion paper [*Wang et al*., 2016]. Figure 2 shows a series of backward trajectory calculations using the Hybrid Single-Particle Lagrangian Integrated Trajectory (HYSPLIT) model [*Draxler and Rolph*, 2003] and covering the majority of the study

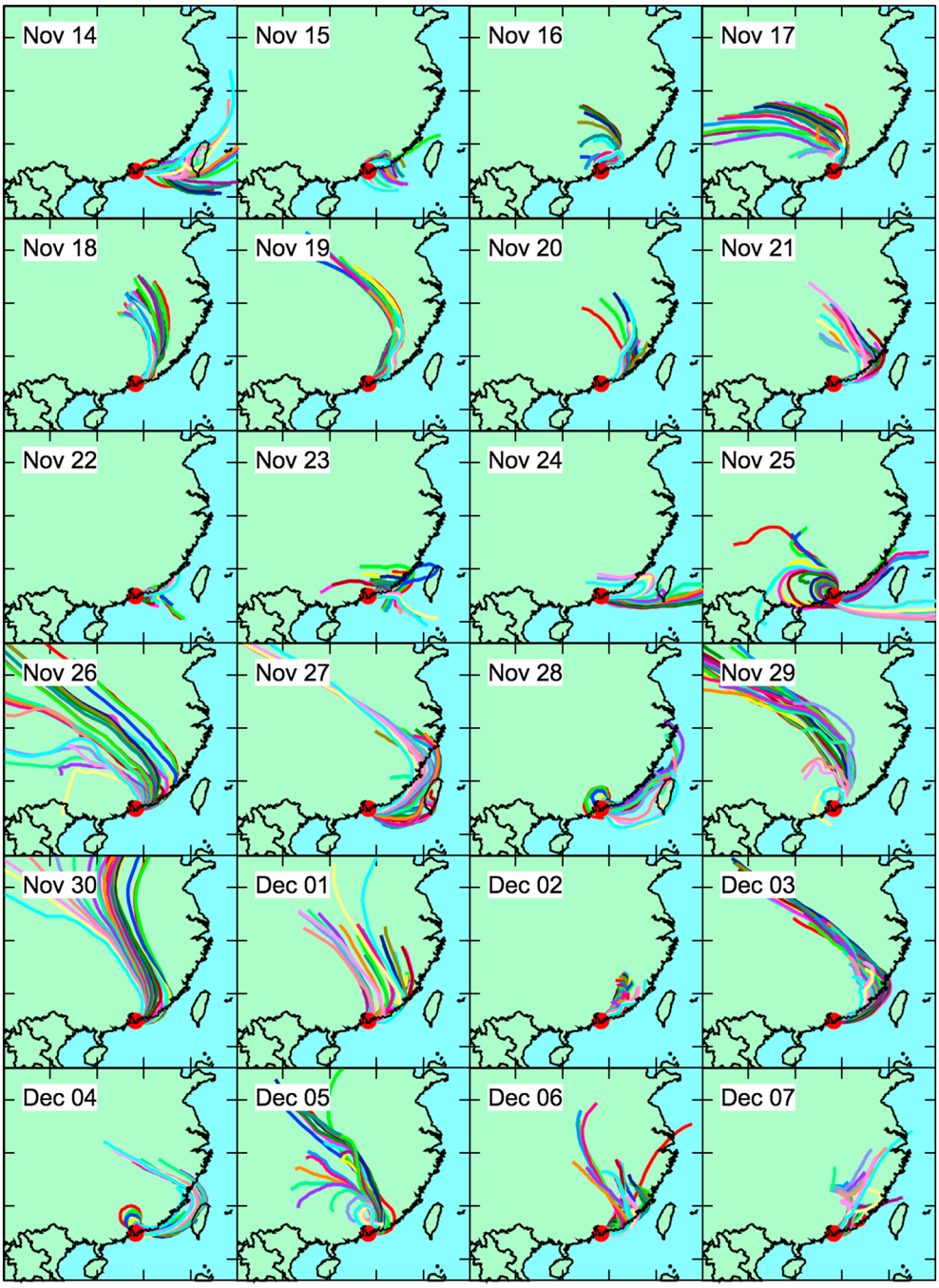


**Figure 2.** Backward trajectory calculations using the HYSPLIT model during the study period. Trajectories are 48 h in duration, initialized every hour at observatory location and 1 km altitude. Trajectories begin at 0Z (8 A.M. local) on the date shown.

period, from 14 November to 7 December 2013. The trajectories are consistent with arrival of air masses from the north and east of the site, but they also clearly show the passage of most air masses over mainland China or Taiwan throughout much of the 48 h of transport on many of the measurement days. The only exceptions are 24–25 November and part of 27 November, when the longer range airflow was distinctly from the east. On these occasions, air at the site had lower $O_3$, higher $NO_x$, and a higher $NO_x$ to $NO_y$ ratio (see below), consistent with entrainment of strong local $NO_x$ emissions from the city of Hong Kong into air with lower $O_3$ transported inward from the South China Sea.

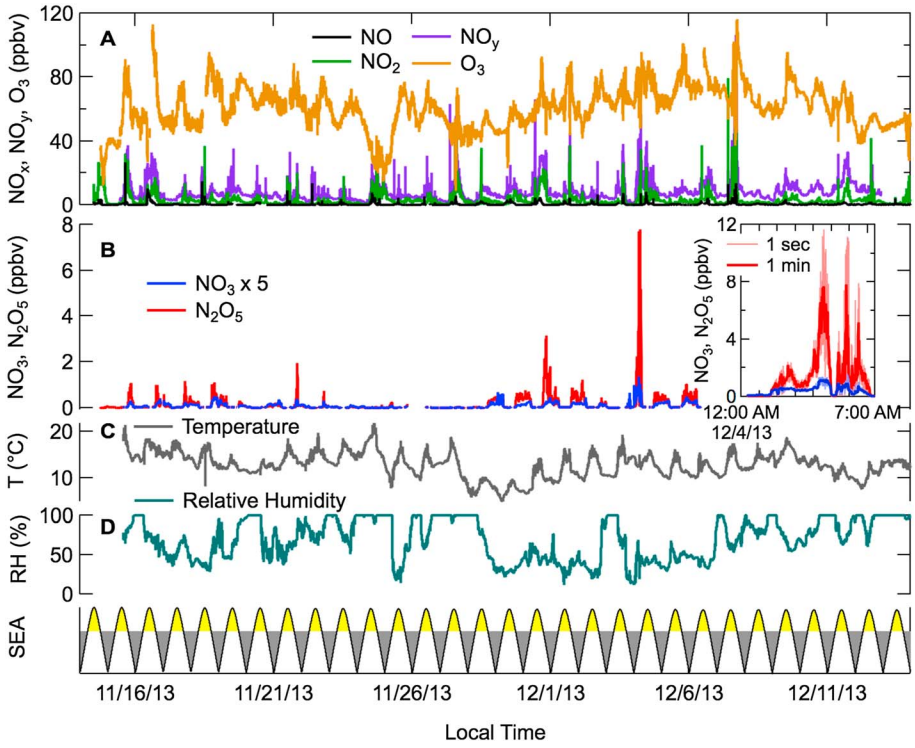


**Figure 3.** Time series of (a) NO, $NO_2$, $NO_y$ and $O_3$; (b) $NO_3$ and $N_2O_5$; (c) temperature; and (d) relative humidity. The bottom plot shows solar elevation angle to reference night and day. Data are at 1 min time resolution. The inset in Figure 3b shows 1 min and 1 s data for the time period from midnight to 7 A.M. on 4 December, when $N_2O_5$ reached its maximum concentration.

The time series of nitrogen oxides and ozone in Figure 3 is consistent with the picture of regionally polluted air at the mountaintop site. Nitrogen oxides ($NO_x$) and total reactive nitrogen ($NO_y$) were variable, as noted above, with a wide range of $NO_x/NO_y$ ratio, indicating a wide range of air mass age sampled at the site. Ozone exhibited characteristic afternoon photochemical peaks, exceeding 80 ppbv in the afternoon on 15 out of 31 days and exceeding 100 ppbv on three days. The nighttime nitrogen oxides, $NO_3$ and $N_2O_5$, were similarly variable. Nightly maximum $N_2O_5$ was in excess of 0.5 ppbv on every night that was not impacted by fog. However, fog was a persistent feature of the site, as shown by the relative humidity time series in Figure 3. Relative humidity (RH) reached 100% for part or all of 16 nights during the entire 31 day study and on 9 of the 21 nights during which $N_2O_5$ was measured with the CRDS instrument. Measured $N_2O_5$ was much lower on foggy nights, especially the period from 22 to 28 November when nightly $N_2O_5$ was nearly always below 0.2 ppbv and frequently below 10 pptv. Levels of $NO_x$ were similar on foggy and nonfoggy nights, suggesting that the lower $N_2O_5$ was due to its rapid loss to heterogeneous uptake in fog droplets.

### 3.1. Diel Averages

Figure 4 shows diel average data for $NO_x$, $NO_y$, and $O_3$. Total reactive nitrogen ($NO_y$) was at its lowest average value between midnight and sunrise (6:47 A.M. campaign average) at 5.8 ppbv but increased steadily throughout the day to a maximum average value of 13.2 ppbv between 16:00 and 17:00. In terms of nitrogen oxidation, air was also most aged between midnight and sunrise, with average $NO_x/NO_y$ of $0.29 \pm 0.03$ ($1\sigma$). The average $NO_x/NO_y$ ratio decreased continuously through the night at a rate of $0.014\,h^{-1}$. The $NO_x/NO_y$ ratio increased during daytime, with the maximum $NO_x/NO_y$ occurring between noon and sunset and an average $NO_x/NO_y$ of $0.41 \pm 0.03$ during daylight hours. The steady rise in $NO_x$ and $NO_y$ throughout the day, together with the increase in the $NO_x/NO_y$ ratio, indicates less aged air sampled at the mountaintop site during daytime, when the boundary layer is presumably well mixed relative to nighttime. At night, the site is likely more isolated from surface emissions.

At the average late night $O_3$ (58 ppbv) and temperature (285 K), the lifetime of $NO_x$ with respect to oxidation via reaction (1) is 4.5–9.0 h, with the longer lifetime corresponding to $1 \times k_1[O_3]$ (where $k_1$ is the rate

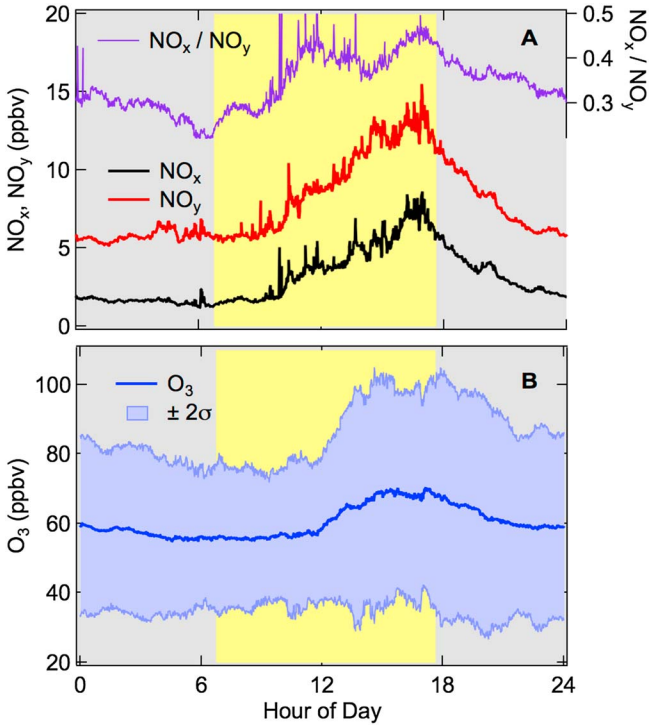


**Figure 4.** Diel average data. (a) $NO_x$, $NO_y$ (left axis), and their ratio, $NO_x/NO_y$ (right axis); (b) $O_3$, with shaded area showing $2\sigma$ variation. Grey and yellow shading on the background indicates the average period of darkness and sunlight, respectively.

coefficient for reaction (1)) and representing the case where $NO_3$ and $N_2O_5$ react mainly through $NO_3$. The shorter lifetime corresponds to $2 \times k_1[O_3]$ and represents reactions mainly through $N_2O_5$ [*Brown et al.*, 2004]. These calculations presume reaction of $NO_3$ with NO to be negligible, which is reasonable for chemistry occurring in the residual layer well removed from direct NO emissions. In the absence of $NO_y$ loss to dry deposition, the average late night $NO_x/NO_y$ ratio is equivalent to an aging time by dark chemistry of 5.5–11 h, i.e., comparable to the duration of a single night. The average nighttime $NO_x/NO_y$ decay rate is, however, considerably slower than that from reaction (1), likely due to averaging of air masses of different photochemical and dark chemistry ages. Comparison of nighttime to daytime oxidation rates requires an estimate of OH radical concentrations, which were not measured or easily constrained by other measurements at this site. For an average daytime OH of $2–5 \times 10^6$, the photochemical lifetime of $NO_2$ would be in the range 5.5–14 h if OH radical reaction with $NO_2$ were the dominant $NO_x$ sink and shorter if other sinks ($NO + RO_2$, PAN formation) were significant [e.g., *Day et al.*, 2003]. The estimated photochemical $NO_x$ lifetime range is comparable to the nocturnal lifetime range.

The diurnal pattern of $O_3$ was typical of that for urban-influenced environments, with a late afternoon maximum of 68.5 ppbv and daily average rise of 12 ppbv. Average $O_3$ did not begin to increase until late morning, with the entire average increase occurring between 11:00 and 15:00. The apparently late onset of $O_3$ photochemistry may indicate that the boundary layer growth containing emissions from the surrounding urban areas does not reach the site until approximately 11 A.M. at this time of year.

### 3.2. High-Concentration, Variable Urban Plumes Sampled at Night

As discussed above, Tai Mo Shan is generally influenced by polluted onshore flow that periodically mixes with continental outflow. A few high-concentration urban plumes whose likely origin was the megacities of the Pearl River Delta region impacted the site at night during discrete events. During these periods, nitrate radical production rates varied from a few tenths to a few ppbv $h^{-1}$, and $N_2O_5$ exhibited periodic large variability (see next paragraph) that was apparent only in data recorded at high time resolution. These characteristics appear to be consistent with infrequent nighttime intercepts of intense pollution plumes at Tai Mo Shan, which is adjacent to but generally not directly downwind of the large megacities of the Pearl River Delta area. High concentrations and large variability may also arise from sampling from a residual layer air mass that has vertically stratified plumes with large spatial gradients [e.g., *Brown et al.*, 2007].

All data in Figure 3 are shown at a time resolution of 1 min except for the inset, which shows the period from midnight to 7 A.M. on 4 December at 1 s resolution. This event had by far the largest $N_2O_5$ concentrations observed during the campaign as well as the largest variability in $N_2O_5$. This maximum $N_2O_5$ is the largest directly measured concentration reported in the literature to date and comparable to $N_2O_5$ levels inferred from measurements of $NO_3$ radicals in the Los Angeles Basin in the late 1970s [*Atkinson et al.*, 1986]. One-minute average $N_2O_5$ exhibited three distinct maxima of 7.7, 7.8, and 5.2 ppbv. During the first two

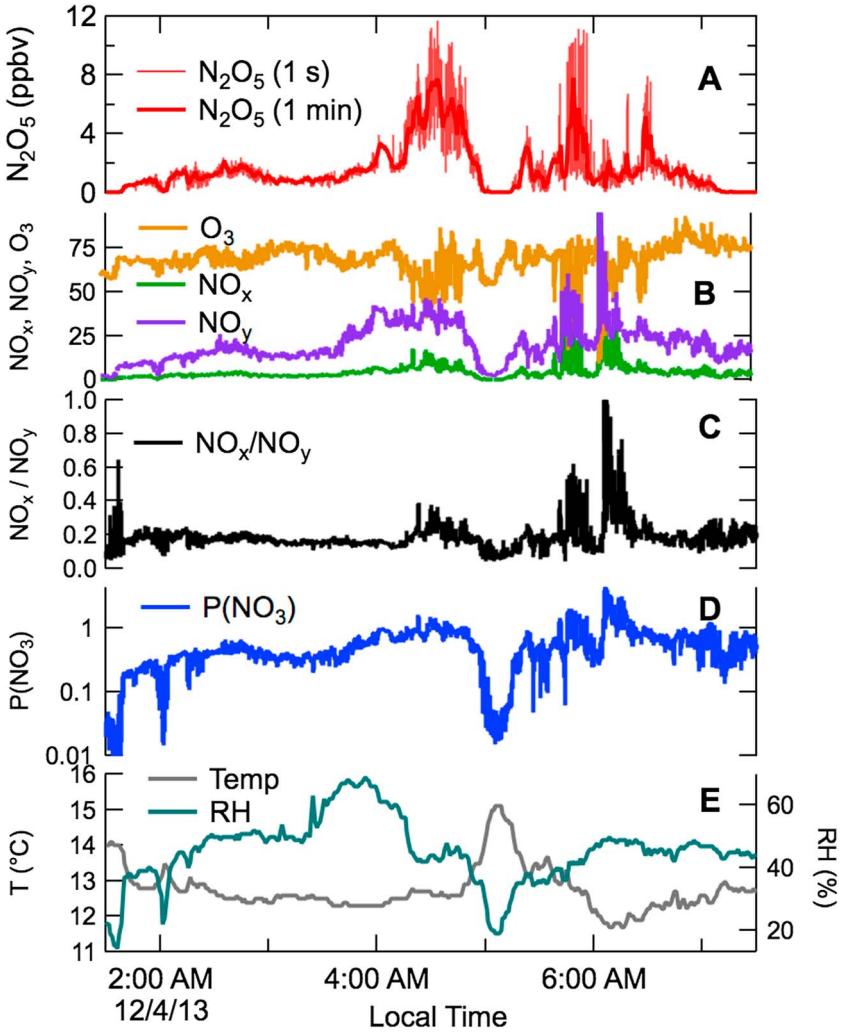


**Figure 5.** Expanded view from 1:30 to 7:30 on 4 December of the time series for (a) $N_2O_5$ at 1 s and 1 min resolution; (b) $O_3$, $NO_x$, and $NO_y$ in ppbv at 1 s resolution; (c, d) $NO_x/NO_y$ and nitrate radical production rate, $P(NO_3)$ in ppbv $h^{-1}$, respectively, at 1 s; and (e) temperature and relative humidity at 1 min.

maxima, 1 s $N_2O_5$ had a standard deviation of 1.5 and 2.7 ppbv, respectively, with relative standard deviations (standard deviation divided by the average) of 19% and 35%. The $N_2O_5$ in the 1 s data reached a maximum mixing ratio of 11.7 ppbv (The CRDS instrument's dynamic range is estimated to be linear up to approximately 100 ppbv).

Variability in the $N_2O_5$ concentrations at the Tai Mo Shan station was accompanied by large variability in $NO_x$ and in air mass age. Figure 5 shows an expanded view of $N_2O_5$, $NO_x$, $NO_y$, $O_3$, the $NO_x$ to $NO_y$ ratio, and the nitrate radical production rate at 1 s time resolution for 1:30–7:30 A.M. on 4 December. Also shown is RH and temperature at 1 min, the best available time resolution for these data. Although the wind was steady from the east (97 ± 3°) with a relatively high wind speed (12.9 ± 0.7 m $s^{-1}$) during the entire period, $NO_3$, $N_2O_5$, $NO_x$, and $NO_y$ varied considerably. Prior to 1:30 A.M. and for a short period just after 5 A.M., temperature was slightly higher and relative humidity considerably lower. The $NO_x$ was low and the air was relatively more aged, with $NO_x/NO_y \sim 0.1$; the production rate of nitrate radicals from reaction (1), $P(NO_3) = k_1[O_3][NO_2]$, was well under 0.1 ppbv $h^{-1}$, approaching 0.01 ppbv $h^{-1}$. These characteristics are consistent with highly aged, polluted air, in which $NO_x$ had been nearly completely oxidized, sampled from above the residual layer. Slightly lower temperature and increased RH after 1:45 A.M. brought $NO_x/NO_y \sim 0.2$ and $P(NO_3)$ of several hundred pptv $h^{-1}$, consistent with a moderately polluted residual layer and moderate nighttime chemistry. Higher $NO_x/NO_y$, increased $P(NO_3)$, and much higher variability in $N_2O_5$ characterized the three large maxima

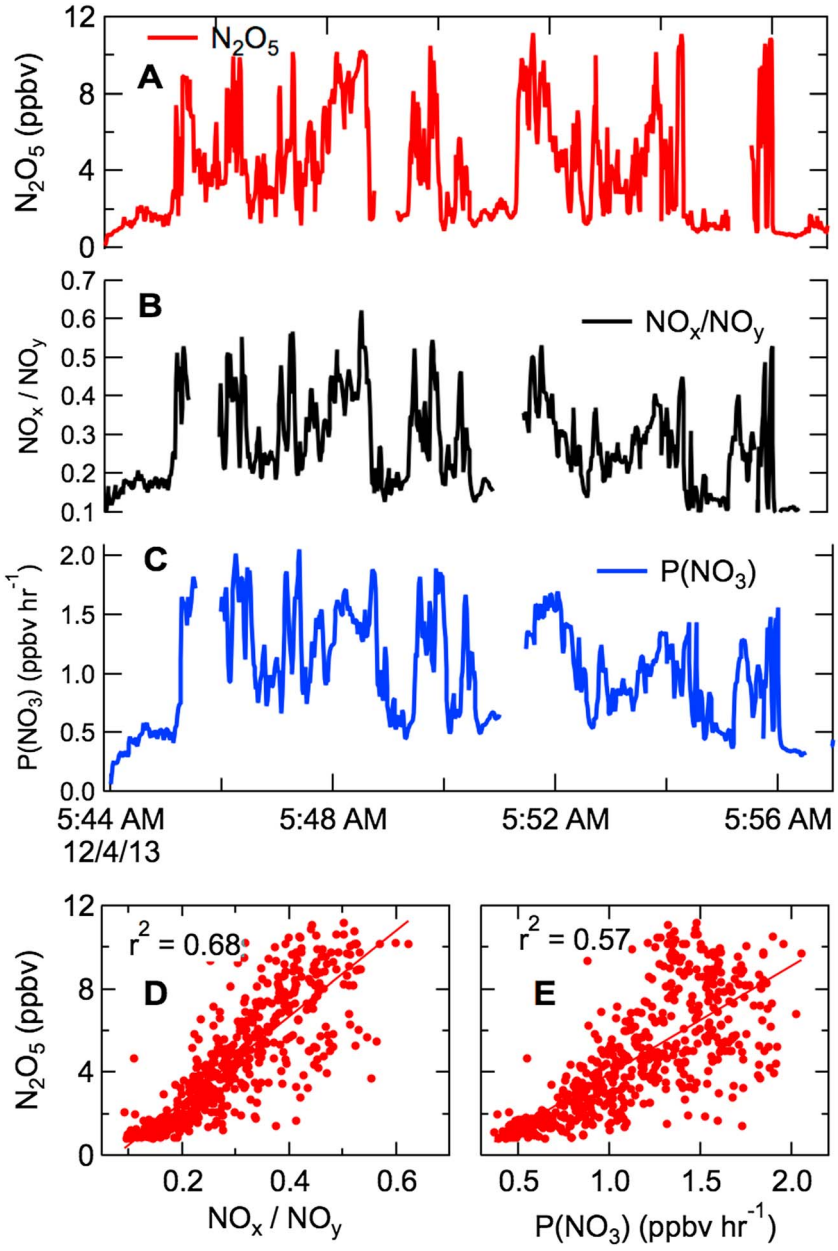


**Figure 6.** Expanded view of the second large $N_2O_5$ plume near 5:45 A.M. from Figure 4 showing (a) $N_2O_5$; (b) $NO_x/NO_y$; (c) $P(NO_3)$; and (d, e) correlations of $N_2O_5$ with $NO_x/NO_y$ and $P(NO_3)$.

in $N_2O_5$ near 4:30, 5:45, and 6:30 A.M. The large increase in $NO_x/NO_y$ and $P(NO_3)$ near 6:15 A.M. did not follow the same pattern and was not accompanied by large $N_2O_5$ but also had $NO_x/NO_y$ near 1, indicative of much more recently emitted $NO_x$ pollution.

Figure 6 illustrates the characteristics of the 5:45 A.M. plume that showed the highest concentrations and the greatest variability in $N_2O_5$. Variabilities in $NO_x/NO_y$ (0.1–0.5) and $P(NO_3)$ (0.5–2.0 ppbv $h^{-1}$) were large and well correlated with variability in $N_2O_5$, indicating that variability in the latter was the result of a rapid shift between $NO_x$-rich and $NO_x$-poor air masses. The correlation of $N_2O_5$ with $NO_x/NO_y$ was slightly better than with $P(NO_3)$, though both were comparable. Sampling of different air masses on a rapid time scale from a mountaintop site could occur if the air pollution plume were confined to a maximum altitude range just equal to the site elevation or if it were transported in a narrow vertical layer. Narrow, vertically layered plumes have been observed, for example, from aircraft measurements of emissions from coal-fired electric power

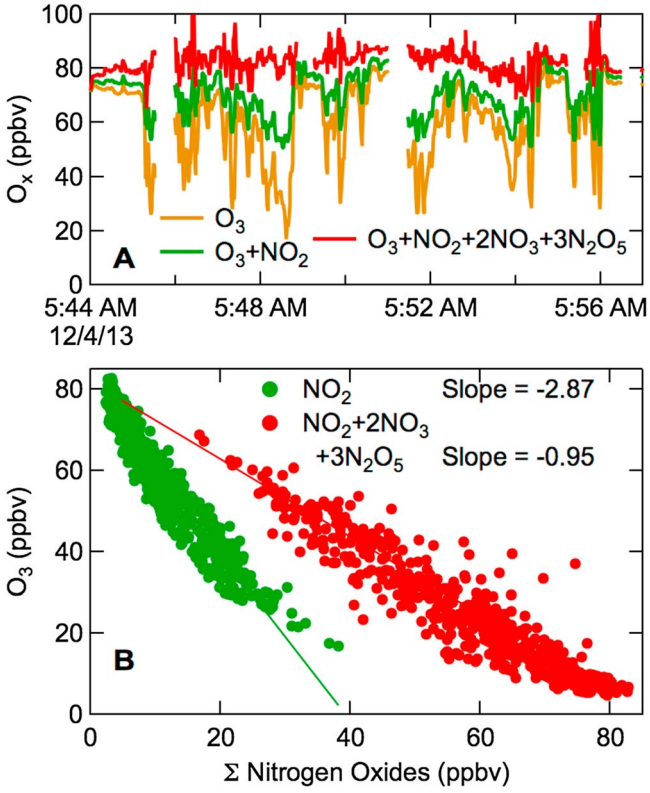


**Figure 7.** Odd oxygen budget for the 5:45 A.M. plume from Figures 4 and 5. (a) Time series of $O_3$, $O_x = O_3 + NO_2$, and nighttime $O_x = O_3 + NO_2 + 2 \times NO_3 + 3 \times N_2O_5$; (b) plots of $O_3$ against $NO_2$ and $NO_2 + 2 \times NO_3 + 3 \times N_2O_5$. The slope of the first plot is a measure of plume age (5.4–7.4 h), while the slope of the second plot is a measure of nighttime $O_x$ conservation (slope near −1 indicates conservation of nighttime $O_x$ in the $N_2O_5$ reservoir).

generation plants in the residual layer [*Brown et al.*, 2007]. The large variability in $N_2O_5$ is similar to that observed previously in Boulder, CO, USA, from a mesa site located on a terrain feature above an urban area [*Brown et al.*, 2003b], similar to Tai Mo Shan but at much lower elevation relative to the nearby urban area. At the Boulder site, variability was shown to arise from large loss rates for $NO_3$ and $N_2O_5$, since the corresponding variability in $NO_2$ and $O_3$, the source gases for $NO_3$ and $N_2O_5$, was small.

As shown in the companion paper [*Wang et al.*, 2016], the highly polluted air mass observed on the night of 4 December came from the Pearl River Delta region based on back trajectories that were calculated with high-resolution wind data simulated by a mesoscale model. Tai Mo Shan, situated to the southeast of Guangzhou and Shenzhen, encounters these plumes infrequently at night, and the large variability may be indicative of the unusual mixing that brings such plumes to this site. Sites situated farther to the west of Tai Mo Shan may encounter large urban plumes during nighttime with greater frequency. Although they are infrequent occurrences at Tai Mo Shan, these intense urban plumes may in fact be characteristic of the nighttime outflow from the Pearl River Delta megacities.

### 3.3. Nocturnal Odd Oxygen

The observation of a large pollution plume exhibiting rapid variability between background and polluted air provides an opportunity to analyze its nocturnal odd oxygen budget. The conventional definition of tropospheric odd oxygen, $O_x$, is the sum of $NO_2$ and $O_3$, since these species rapidly interconvert photochemically. Nocturnal odd oxygen also includes $NO_3$ and $N_2O_5$ in their stoichiometric ratio with the number of $O_3$ molecules required to form each compound through reactions (1) and (2) [*Brown et al.*, 2006a].

$$O_x = NO_2 + O_3 \tag{6}$$

$$\text{Nocturnal } O_x = NO_2 + O_3 + 2NO_3 + 3N_2O_5 \tag{7}$$

Figure 7a shows $O_3$, $O_x$, and nocturnal $O_x$ for the 4 December 5:45 A.M. plume. Whereas $O_3$ and $O_x$ show large variability, similar to that seen in $N_2O_5$, $NO_x/NO_y$, and $P(NO_3)$, nocturnal $O_x$ is approximately constant across the entire plume intercept. This behavior indicates a nighttime emitted plume that did not undergo photochemical $O_3$ production but rather only $O_3$ consuming reactions during darkness. Figure 7b shows a plot of $O_3$ against $NO_2$ and against the sum of nitrogen oxides in their stoichiometric ratio to $O_3$, i.e., $NO_2 + 2NO_3 + 3N_2O_5$. Ozone and $NO_2$ are tightly anticorrelated. If the majority of the $NO_x$ emissions had occurred in the form of NO (i.e., little primary $NO_2$), a fit of $O_3$ against $NO_2$ should yield a slope close to −1 if no nighttime $NO_2$ oxidation had occurred. Slopes steeper than this value indicate the further nighttime oxidation of $NO_2$. This nocturnal relationship between $O_3$ and $NO_2$ is a chemical clock defined by the rate coefficient for reaction (1) with an analytically simple, linear expression that is accurate as long as $O_3$ is in excess of $NO_2$

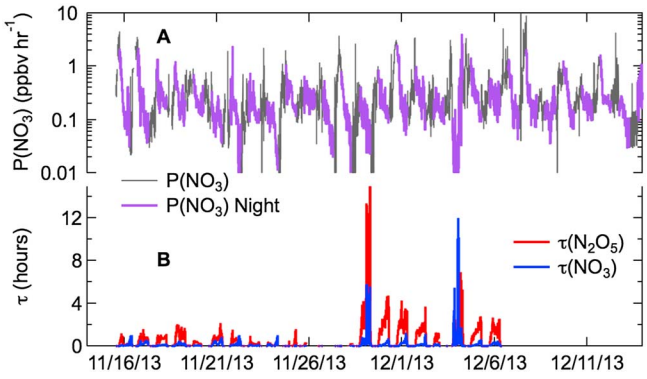


**Figure 8.** Time series of (a) $NO_3$ production rate, with heavier purple overlay indicating nighttime data and (b) $N_2O_5$ and $NO_3$ lifetimes.

[*Brown et al.*, 2006a]. To satisfy this condition, the fit is only for the initial portion of the $O_3$ versus $NO_2$ plot between 60 and 80 ppbv, yielding a slope of −2.87. Conversion of this slope to a processing time depends on the fate of $NO_3$ and $N_2O_5$ (i.e., loss through $NO_3$, loss through $N_2O_5$, or a stable reservoir) but gives a range of 5.4–7.4 h. Although the local wind speed and direction indicated steady transport from the east or northeast, the high-resolution transport analysis in the companion paper [*Wang et al.*, 2016] indicates that the urban pollution in this plume originated in the Pearl River Delta area of mainland China. Because the prevailing wind at this site normally did not pass over the urban areas of this region, intercepts of pollution from this region were infrequent. However, it is likely that the urban plumes from the Pearl River Delta undergo significant nighttime chemistry within the residual layer with substantial mixing ratios of both $N_2O_5$ and $ClNO_2$.

The constant $O_x$ in Figure 7a and the slope near −1 for $O_3$ versus $NO_2 + 2NO_3 + 3N_2O_5$ in Figure 7b indicates that most of the odd oxygen consumed through reactions (1) and (2) is conserved in the form of a stable reservoir of $N_2O_5$, assuming that there is no influence of surface level NO emissions during transport within the residual layer at the sampled altitude during the night. Uptake of $N_2O_5$ evidently was relatively slow in this plume, whose relative humidity was 42%.

## 4. Reactivity and Lifetimes of $NO_3$ and $N_2O_5$

Both $NO_3$ and $N_2O_5$ are reactive intermediates that undergo reactions with volatile organic compounds and heterogeneous uptake to aerosol, respectively. The relative rates of these sink reactions are important to understanding the principal reaction products from nighttime chemistry and their influence on reactive nitrogen, ozone, and aerosols. The steady state lifetimes of $NO_3$ and $N_2O_5$, $\tau(NO_3)$, and $\tau(N_2O_5)$, are the ratio of their observed mixing ratios to the nitrate radical production rate, $P(NO_3)$, and are commonly used measures of their reactivity [*Brown et al.*, 2003a; *Platt et al.*, 1984].

$$\tau(NO_3) = \frac{NO_3}{k_1 O_3 NO_2}; \quad \tau(N_2O_5) = \frac{N_2O_5}{k_1 O_3 NO_2} \tag{8}$$

Figure 8 shows the time series of $P(NO_3)$ (log scale), $\tau(NO_3)$, and $\tau(N_2O_5)$. Nitrate radical production rates (1 min averages) varied over more than 3 orders of magnitude, from less than 0.01 ppbv $h^{-1}$ to 10 ppbv $h^{-1}$, with an average value of 0.32 ppbv $h^{-1}$. Nitrate radical production rates tended to peak in late afternoon, concurrently with the maximum in $NO_x$ and $O_3$, and then decrease slowly during the night. Thus, the most active period for nighttime chemistry, at least in terms of radical production rates, was during early evening just after sunset. Nighttime average $P(NO_3)$ was slightly lower, at 0.26 ppbv $h^{-1}$. Lifetimes of $NO_3$ and $N_2O_5$ varied from <0.1 to 13 h, although the very long lifetime events corresponded to low production rates and small denominators in equation (8) rather than large mixing ratios of $NO_3$ and $N_2O_5$. Under more polluted conditions typical of the majority of the data, nightly maximum $N_2O_5$ lifetimes varied over the range 1–2 h during the first half of the campaign (15–26 November) and 2–5 h in the second half (28 November to 6 December). Relative humidity was higher during the first period (73 ± 22%) than during the second (45 ± 19%). The $N_2O_5$ lifetime showed a clear dependence on relative humidity (Figure 9), consistent with its heterogeneous uptake in reactions (4) and (5) playing a large role as a sink reaction. Its lifetime varied from a median above 2 h at 25% RH to 0.3 h at 95% RH. A part of this difference may be due to increased aerosol surface area due to hygroscopic aerosol growth at higher RH, and a part may be due to an RH dependence of the $N_2O_5$ uptake coefficient [*Brown and Stutz*, 2012]. Figure 9b shows the dependence of $\tau(N_2O_5)$ on aerosol surface area, which includes hygroscopic growth. The lifetime decreases with

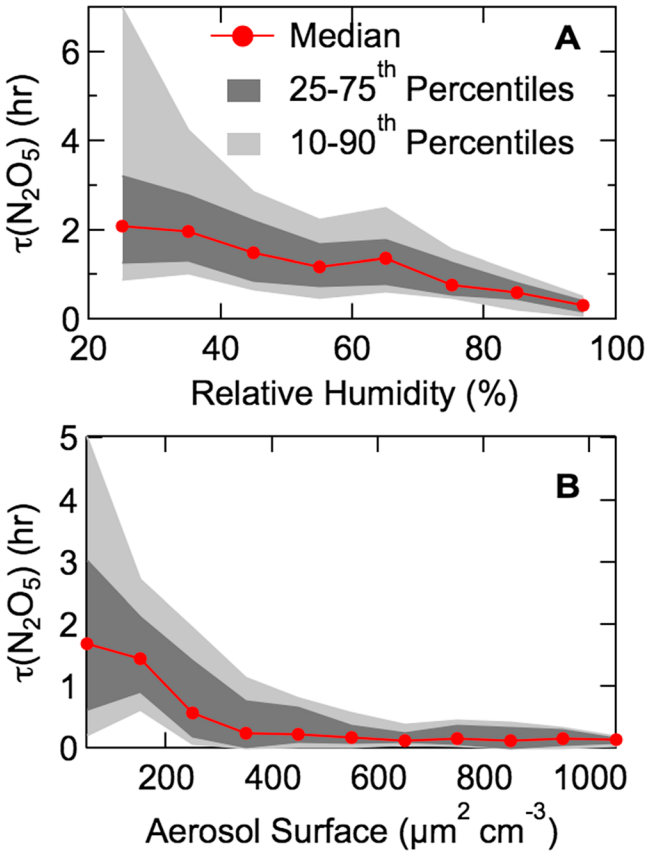


**Figure 9.** $N_2O_5$ lifetime from 3 h past sunset until sunrise versus (a) relative humidity, binned in increments of 10% and (b) aerosol surface area, binned in increments of 100 $\mu m^2$ $cm^{-3}$. Data are shown as medians, 25–75th percentile ranges, and 10–90th percentile ranges, as shown in the legend.

increasing surface area up to 500 $\mu m$ $cm^{-3}$ but is approximately constant thereafter. The large majority (85%) of the data occurred at surface areas smaller than this threshold, however. The trend in $\tau(N_2O_5)$ with aerosol surface area may arise either from increased $N_2O_5$ uptake rates at higher available surface area or with increased rates of $NO_3$-VOC reactions in more polluted air with larger aerosol loads.

### 4.1. Individual Sinks for $NO_3$ and $N_2O_5$

Because $NO_3$ and $N_2O_5$ are in rapid thermal equilibrium, the individual sinks for either compound contribute to the removal of the pair. The dependence of the steady state lifetime on $NO_2$, which determines the ratio of $NO_3$ and $N_2O_5$ and thus the relative importance of the reactions of either to the loss of the pair, is one method for separating the individual contributions of $NO_3$ reactions and $N_2O_5$ heterogeneous uptake [*Brown et al.*, 2003a]. This method has been demonstrated for sampling within the residual layer during transects of individual $NO_x$ plumes sampled aloft from aircraft [*Brown et al.*, 2006b; *Brown et al.*, 2009]. A linear form of this relationship that gives the $N_2O_5$ uptake coefficient, $\gamma(N_2O_5)$ as the slope, and the first-order loss rate coefficient for $NO_3$, $k(NO_3)$ as the intercept, is as follows [*Brown et al.*, 2009].

$$\tau(N_2O_5)^{-1}K_{eq}[NO_2] = k(NO_3) + \frac{1}{4}cS_AK_{eq}[NO_2]\gamma(N_2O_5) \quad (9)$$

Here $K_{eq}$ is the temperature-dependent equilibrium coefficient for the $NO_3$-$N_2O_5$ equilibrium in reaction (2), $c$ is the mean molecular speed of $N_2O_5$, and $S_A$ is the aerosol surface area. Figure 10 shows an example plot of $\tau(N_2O_5)^{-1}K_{eq}[NO_2]$ versus $\frac{1}{4}cS_AK_{eq}[NO_2]$ for 20–21 November. Although an equation similar to (9) can be written for $\tau(NO_3)$, the $NO_3$ measurement was not independent of $N_2O_5$ for this data set, and only the $N_2O_5$ plot is shown. Equation (9) is approximately valid if $NO_3$ and $N_2O_5$ have achieved steady state, i.e., if $dNO_3/dt$ and $dN_2O_5/dt$ are both approximately 0. Steady state lifetimes increased continuously on many nights during approximately the first 3 h after sunset, indicating an approach to steady state of approximately this duration. Data in Figure 10 and for determinations from other nights therefore exclude the first 3 h of data. Previous analysis of aircraft measurements in other locations has shown that $S_A$ exhibits a positive, linear correlation with $NO_2$ and that this covariance can be accounted for by explicit inclusion of $S_A$ in equation (9) [*Brown et al.*, 2009]. Covariance may also occur between $NO_2$ and $k(NO_3)$. A positive covariance between these quantities would increase the slope and decrease the intercept of the linear fit, leading to an overestimate of $\gamma(N_2O_5)$ and an underestimate of $k(NO_3)$. Indeed, fits to the data on several nights produced negative values for $k(NO_3)$, potentially as a result of this covariance. Table 1 shows $\gamma(N_2O_5)$ and $k(NO_3)$ derived from similar fits to 10 nights of the campaign. Nights with negative $k(NO_3)$ were excluded. Data were also filtered for RH $<$ 90% due to the uncertainty in the aerosol surface area at high RH [*Wang et al.*, 2016]. Averaged across all nights on which the determination was possible, $\gamma(N_2O_5) = 0.014 \pm 0.007$ and $k(NO_3) = 5.6 \pm 2.5 \times 10^{-4}$ $s^{-1}$.

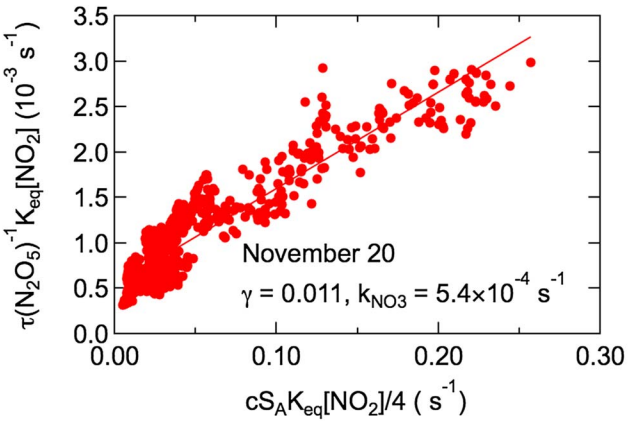


**Figure 10.** Example fit of $N_2O_5$ lifetime according to equation (9) for data from the night of 20–21 November.

Because of the potential covariance described above, these values are simply the best fits for $\gamma(N_2O_5)$ and $k(NO_3)$ to within these limitations. They do not account for potential variability in these quantities but do represent the average values of these parameters that best describe the steady state lifetimes of the observed data. The derived $\gamma(N_2O_5)$ lie within the range of 0.002–0.04 from previous field-based determinations from aircraft or tall tower sampling in the residual layer, which generally range from 0.001 to 0.04 [*Brown et al.*, 2006b, 2009; *Wagner et al.*, 2013]. The $k(NO_3)$ are low, corresponding to a nighttime $NO_3$ lifetime in excess of 30 min. Low average $NO_3$ reactivity is consistent with measurement in relatively aged air within the residual layer depleted in reactive VOCs.

Figure 11 shows a diel average of $\tau(N_2O_5)$ from equation (8) (black line) for all data with RH < 90%. (The large plumes of $N_2O_5$ do not exhibit lifetimes that are as much larger as the $N_2O_5$ mixing ratios themselves and thus do not bias the diel averaged lifetime.) Also shown on the plot is the calculated $N_2O_5$ lifetime for three cases. Calculated lifetimes are derived from equation (9) as follows.

$$\tau(N_2O_5)_{Calc} = \left[\frac{k(NO_3)}{K_{eq}[NO_2]} + \frac{1}{4}cS_A\gamma(N_2O_5)\right]^{-1} \quad (10)$$

Calculated lifetimes are shown continuously throughout the diel cycle but are only comparable to the observations at night. Case 1 (green line) represents all reactivity of $NO_3$ and $N_2O_5$ attributed to $N_2O_5$ uptake. In this case, the uptake coefficient that best matches the data from 3 h past sunset until sunrise (average lifetime of 1.6 h) is $\gamma(N_2O_5) = 0.023$. Conversely, case 2 (blue line) shows the predicted lifetime if all reactivity were attributable to $NO_3$, i.e., for $\gamma(N_2O_5) = 0$. In this case $k(NO_3)$ is $1.4 \times 10^{-3}$ $s^{-1}$ or a lifetime of approximately 12 min. The large peak in $\tau(N_2O_5)_{calc}$ just before sunset for this case is due to the peak in $NO_x$ at that time (see Figure 4), which leads to a maximum in $K_{eq}[NO_2]$ and in $\tau(N_2O_5)_{calc}$ for $\gamma(N_2O_5) = 0$ using equation (10) (i.e., $\tau(N_2O_5)_{calc}$ proportional to $NO_2$). Case 3 (red line) shows $\tau(N_2O_5)_{calc}$ for the parameters derived from the average of the nightly fits to the steady state lifetime dependences, $\gamma(N_2O_5) = 0.014$ and $k(NO_3) = 5.6 \times 10^{-4}$. This case is intermediate between the extremes and fits the nighttime average $\tau(N_2O_5)$ equally well. Average $\tau(N_2O_5)$ between 4:00 and 6:30 A.M. is somewhat greater. An uptake coefficient $\gamma(N_2O_5) = 0.005$ approximately fits the data during this time period using $k(NO_3) = 5.6 \times 10^{-4}$ $s^{-1}$.

Figure 11b shows the average magnitude of loss via $NO_3$ (blue) and $N_2O_5$ (red), i.e., the two terms on the right-hand side of equation (10), using the average uptake coefficients and $NO_3$ loss rate coefficient. The

**Table 1.** $N_2O_5$ Uptake Coefficients and $NO_3$ Loss Rate Coefficients From a Nightly Steady State Analysis

| Date | $\gamma(N_2O_5)$ | $k(NO_3)$ ($10^{-4}$ $s^{-1}$) |
|---|---|---|
| 16–17 November | 0.022 | 5.6 |
| 17–18 November | 0.014 | 5.8 |
| 18–19 November | 0.0075 | 4.6 |
| 19–20 November | 0.015 | 8.1 |
| 20–21 November | 0.011 | 5.4 |
| 21–22 November | 0.029 | 4.3 |
| 30 November 30 to 1 December | 0.0075 | 4.9 |
| 1–2 December | 0.021 | 1.7 |
| 2–3 December | 0.010 | 11 |
| 3–4 December | 0.004 | 4.1 |

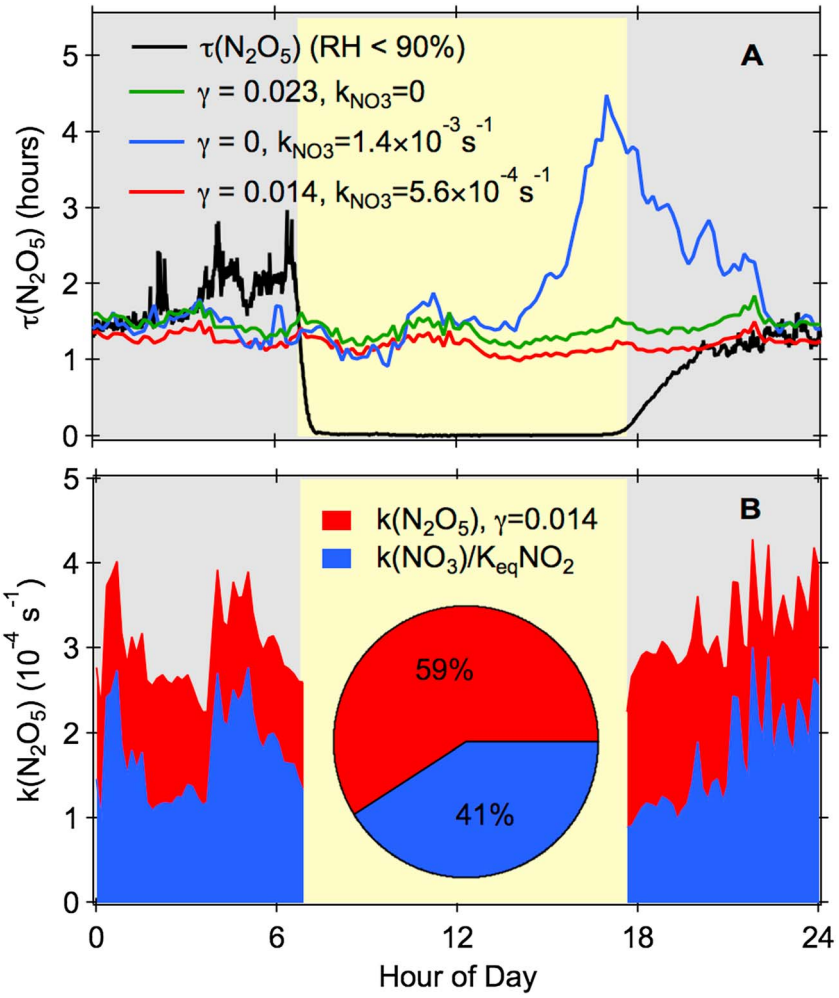


**Figure 11.** (a) Diel average $N_2O_5$ lifetime for RH < 90% (black). Also shown are calculated $N_2O_5$ lifetimes that best match the average for the case of sinks of $N_2O_5$ only (green), sinks of $NO_3$ only (blue), and the average of the nightly determinations of $\gamma(N_2O_5)$ and $k(NO_3)$ (red). The legend gives corresponding uptake coefficients and $k(NO_3)$. Calculated values show both daytime and nighttime data, although photochemical reactions of $NO_3$ dominate the daytime sinks. (b) Average nighttime loss rate coefficients for $NO_3$ and $N_2O_5$ using the average nightly $\gamma(N_2O_5)$ and $k(NO_3)$. The $k(NO_3)$ is divided by $K_{eq}[NO_2]$ for direct comparison to $k(N_2O_5)$ (see text). Pie chart in the center shows relative contribution of $N_2O_5$ and $NO_3$ sinks.

pie chart in the center of the figure gives the relative contribution of each. They are nearly equal, although $N_2O_5$ loss accounts for slightly more than half of the total.

### 4.2. $NO_3$ Reactivity From Daytime Canister Samples

The first-order loss rate coefficient for $NO_3$ determined from the nighttime $N_2O_5$ lifetime analysis can be compared with that determined from measurements of reactive VOCs at the Tai Mo Shan observatory during daytime. The VOC canister measurements were not automated, and nighttime site access restrictions prevented their collection during darkness. A total of 38 canister samples were collected from 27 November to 13 December. Figure 12 shows the average $NO_3$ first-order loss rate coefficients, $k(NO_3)$, sorted by anthropogenic and biogenic hydrocarbons. The $k(NO_3)$ were calculated from the sum of the products of the bimolecular rate coefficients for reactions of VOCs with $NO_3$ and the VOC concentrations.

$$k(NO_3) = \sum_i k(NO_3 + VOC_i)[VOC_i] + K_{eq}[NO_2]k(N_2O_5) \quad (11)$$

The second term on the right-hand side of equation (11) is the $NO_3$ first-order loss rate coefficient through uptake of $N_2O_5$ [*Brown et al.*, 2003a], shown as the black bar at the bottom of Figure 12 for reference.

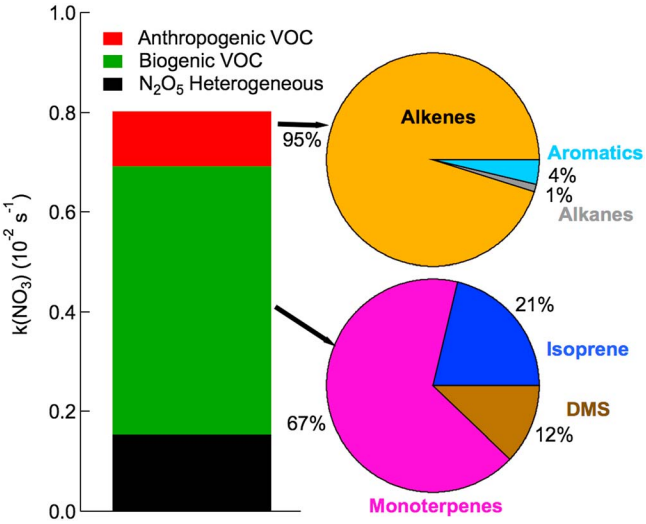


**Figure 12.** $NO_3$ reactivity measured from canister samples acquired during daytime. (left) Bar graph shows the average $NO_3$ summed first-order loss rate coefficient with biogenic and anthropogenic VOCs together with its loss through $N_2O_5$ uptake using an uptake coefficient of $\gamma(N_2O_5) = 0.014$. (right) Pie charts show the contributions of different categories of VOC to the anthropogenic (top) and biogenic (bottom) components. The $k(NO_3)$ from daytime canister samples is approximately 10 times larger than that inferred from nighttime $N_2O_5$ lifetimes.

Average daytime $k(NO_3)$ from VOC measurements (excluding loss through $N_2O_5$) was $6.5 \pm 6.8 \times 10^{-3}$ $s^{-1}$, equivalent to an $NO_3$ lifetime of approximately 2.5 min and more than 10 times the average $k(NO_3)$ derived from the nighttime steady state analysis. The much faster $NO_3$ loss rate is consistent with a substantially less aged air mass that was more influenced by surface level emissions sampled at the mountaintop site during the daytime mixed boundary layer than during the nighttime residual layer. The pie charts on the right-hand side of Figure 12 show the VOC categories that made up the reactivity. Anthropogenic $NO_3$-VOC reactivity was $1.1 \pm 1.9 \times 10^{-3}$ $s^{-1}$, twice the total nighttime $NO_3$ reactivity, and was dominated by anthropogenic alkenes, such as propene and butenes. Aromatics and alkanes made a minor contribution (5%) total. This distribution of $NO_3$ reactivity with anthropogenic VOCs is similar to that from urban areas in the U.S. [*Brown et al.*, 2011]. Monoterpenes were the dominant component of $NO_3$-biogenic VOC reactivity, with α- and β-pinene being the only two reported compounds.

Daytime VOC measurements clearly did not reflect the $NO_3$ reactivity that occurred during the majority of the night but may be indicative of the chemistry occurring during the early hours of the evening during the approximately 3 h time period required for the approach to steady state described above.

## 5. Daytime $N_2O_5$

Although $NO_3$ and $N_2O_5$ normally occur in large concentrations only at night in the lower troposphere, they are present at small but nonzero levels during daytime. Several studies have reported measurements of daytime $NO_3$ or $N_2O_5$ from ground sites [*Geyer et al.*, 2003], ships [*Osthoff et al.*, 2006], and aircraft [*Brown et al.*, 2005] in the U.S., as well as from a lower altitude site in Hong Kong [*Wang et al.*, 2014]. During the 2013 Tai Mo Shan study, the largest $NO_x$ and least aged urban emissions occurred during late afternoon (Figure 4) and early evening, such that the largest $P(NO_3)$ and potentially most active $NO_3$ and $N_2O_5$ chemistry occurred during this time of day. Figure 13 shows the diel average $N_2O_5$ plotted on a logarithmic scale to illustrate the small but nonzero daytime mixing ratio, which varied between 1 and 2 pptv between 9:00 and 14:00. From 14:00 to 19:00, $N_2O_5$ mixing ratios rose continuously to an average maximum of ~350 pptv near 19:00, with an average sunset mixing ratio of ~60 pptv. Also shown in Figure 13 is the calculated daytime $N_2O_5$ predicted from a steady state between production through reactions (1) and (2) and loss through $NO_3$ photolysis and reaction with NO (reactions (12) and (13) below).

$$NO_3 + h\nu \rightarrow \text{products}(NO_2 + O \text{ or } NO + O_2) \quad (12)$$

$$NO_3 + NO \rightarrow 2NO_2 \quad (13)$$

The rate coefficient for reaction (13) is rapid ($k = 2.6 \times 10^{-11}$ $cm^3$ $molecule^{-1}$ $s^{-1}$ at 298 K [*Sander et al.*, 2011]), such that reaction (13) is more rapid than $NO_3$ photolysis in determining daytime levels of $NO_3$ and $N_2O_5$ for NO above approximately 0.3 ppbv. If other loss processes for $NO_3$ and $N_2O_5$ are small compared to reactions (12) and (13), equation (14) gives the predicted daytime steady state in $N_2O_5$ [*Brown et al.*, 2005].

$$N_2O_5(\text{Day}) = K_{eq}[NO_2]\frac{P(NO_3)}{j(NO_3) + k_{13}[NO]} \quad (14)$$

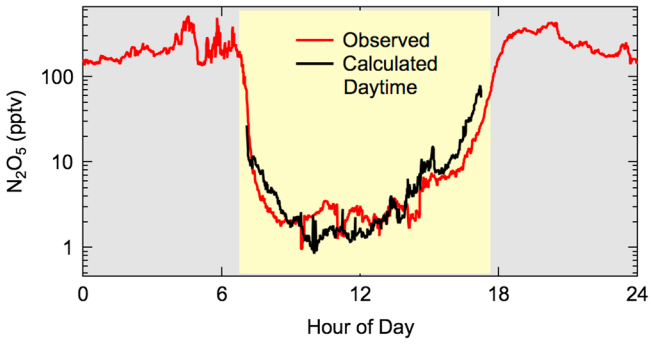


**Figure 13.** Diel average $N_2O_5$ on a logarithmic scale (red) together with a calculation of daytime (solar elevation angle > 5°) average $N_2O_5$ according to equation (14).

Here $j(NO_3)$ is the first-order photolysis rate coefficient for reaction (12), for which there were no direct measurements. Photolysis rate coefficients for $NO_2$ were measured, and $j(NO_3)$ was calculated based on its correlation with $j(NO_2)$ from aircraft data during the TexAQS 2006 campaign [*Parrish et al.*, 2008]. The estimated error in deriving $j(NO_3)$ from this correlation is ±30%. The black line in Figure 13 shows the average calculated daytime $N_2O_5$ (arbitrarily defined here as solar elevation angle > 5° to avoid periods near dawn and dusk) for comparison to observation. The calculation has the same pattern as the observations and is of the same magnitude (1–2 pptv) through the morning and early afternoon hours. During the late day rise in $N_2O_5$, the calculation overpredicts the observation, possibly indicating that sinks other than reactions (12) and (13) are important during late afternoon, when $NO_3$ production rates are largest.

Figure 14 shows the same comparison for two individual days, 27 November and 30 November, to illustrate the influence of daytime $N_2O_5$ heterogeneous uptake. Both days had large afternoon $P(NO_3)$. On 30 November there was sustained $P(NO_3)$ of 2–3 ppbv $h^{-1}$, while 27 November had $P(NO_3)$ of 1–2 ppbv $h^{-1}$ with a sharp maximum above 3.5 ppbv $h^{-1}$. On 30 November, the observed and calculated late afternoon $N_2O_5$ values agree well, with the observations on average 80% of the calculation (i.e., observations 20% lower than the calculation) between 14:00 and sunset. On 27 November, by contrast, observations are much smaller, adding up to only 5% of the calculation during the same period of the day, suggesting that 95% of the $NO_3$ and $N_2O_5$ sinks were other than reactions (12) and (13). Relative humidity was saturated at 100% on 27 November, indicating that the site was impacted by fog at that time. Uptake of $N_2O_5$ to fog droplets is thus a likely candidate for the discrepancy [*Lelieveld and Crutzen*, 1990]. If the dominant (95%) loss process for $N_2O_5$ during this late afternoon event were

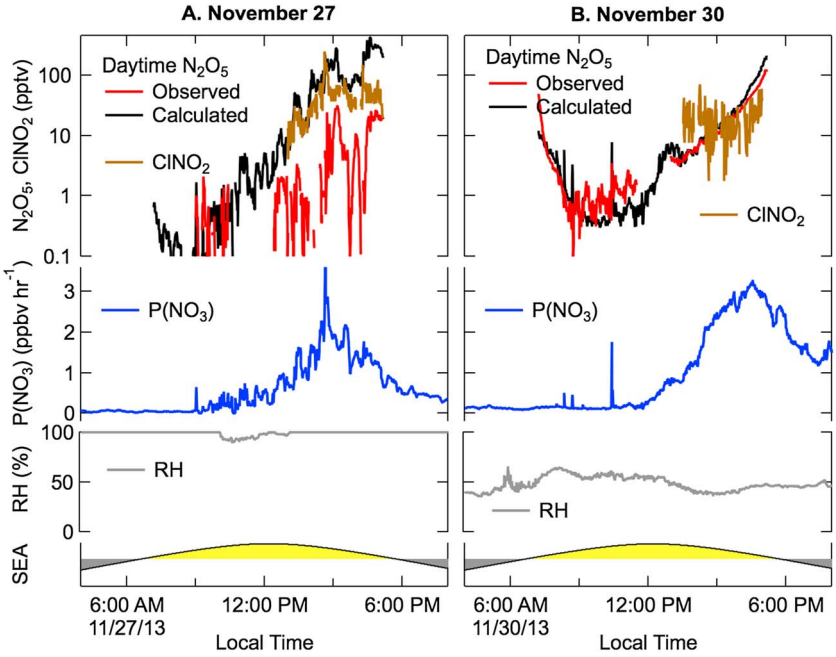


**Figure 14.** Observed and calculated daytime $N_2O_5$ and observed $ClNO_2$ (for the time period when these data were available), nitrate radical production rate, and relative humidity for (a) 27 November and (b) 30 November. Bottom plots show solar elevation angle (SEA) for reference of day and night.

through heterogeneous uptake, the resulting conversion of $NO_x$ to soluble nitrate and/or $ClNO_2$ would proceed at twice the nitrate radical production rate, or 2.7 ppbv $h^{-1}$. For reference, reaction of OH with $NO_2$ at the observed concentration would proceed at approximately 1 ppbv $h^{-1}$, assuming a late afternoon OH concentration of $2 \times 10^6$ $cm^{-3}$. Thus, daytime production of soluble nitrate via $N_2O_5$ can be substantially faster than photochemical conversion through $OH + NO_2$ in the polluted clouds that impact this mountaintop observatory.

Figure 14 also shows the $ClNO_2$ product from $N_2O_5$ uptake during daylight hours for both days. On the high RH/fog day, $ClNO_2$ follows calculated $N_2O_5$ production and significantly exceeds $N_2O_5$ itself. The apparent agreement between $ClNO_2$ and calculated $N_2O_5$ is fortuitous, however, since there is no daytime steady state in $ClNO_2$ that is analogous to $N_2O_5$. Rather, $ClNO_2$ more nearly represents its integrated production. At an average afternoon mixing ratio of 50 pptv, $ClNO_2$ is likely much smaller than soluble nitrate, which would be produced rapidly at the rate given above. The observation of a small $ClNO_2$ mixing ratio under conditions of rapid nitrate production via $N_2O_5$ is consistent with a small $ClNO_2$ yield in fog droplets that consist mainly of water [*Bertram and Thornton*, 2009; *Roberts et al*., 2009]. On the low-RH day, $ClNO_2$ is present at a mixing ratio approximately equal to or smaller than that of $N_2O_5$, likely as the result of much less rapid $N_2O_5$ heterogeneous uptake but potentially larger $ClNO_2$ yield. Daytime heterogeneous chemistry of $N_2O_5$ may therefore be a small source of photolabile chlorine under both dry and wet conditions, although it would provide a large source of soluble nitrate in wet but not dry conditions. The companion paper presents a much more extensive analysis of the nighttime characteristics of $ClNO_2$ and its influence on next-day photochemistry [*Wang et al*., 2016].

## 6. Conclusions

We report the first observations of the nighttime nitrogen oxides, $NO_3$ and $N_2O_5$, from a site in the residual layer in China. Observations took place at Tai Mo Shan, a mountaintop observatory in Hong Kong and within the Pearl River Delta region. Although the site was high enough (957 m) to periodically sample from above the daytime mixed boundary layer, it was always influenced by at least moderate $NO_x$ pollution. Maximum nightly mixing ratios of $N_2O_5$ were generally in the range of 0.5–4 ppbv on nights without significant influence of fog but were observed at 7.8 ppbv (1 min average) and 11.8 ppbv (1 s average) during one large event. The event exhibited large variability observable in measurements with 1 s time resolution and possibly driven by sampling from a poorly mixed air pollution plume advecting over the mountaintop site. Although intense urban pollution events were infrequent at Tai Mo Shan due to the prevailing easterly air flow at this site, the large nighttime plume intercepts were likely indicative of the typical characteristics of nighttime urban outflow from the megacities of the Pearl River Delta.

Analysis of the $NO_x$ and aerosol dependence of the $N_2O_5$ steady state lifetime yielded an average uptake coefficient to aerosol of $\gamma(N_2O_5) = 0.014 \pm 0.007$, although the uncertainty does not likely represent the full range of potential variability in this uptake coefficient. This number is likely an upper limit due to potential artifacts in the determination method. Nighttime average $NO_3$ loss rate coefficients were determined to be slow, equivalent to an $NO_3$ lifetime longer than 30 min in aged air sampled at the mountaintop site. Even with the slower loss rate coefficient for $NO_3$, sinks of $NO_3$ and $N_2O_5$ each contributed approximately equally to the total loss rate of the pair of compounds. Analysis of $NO_3$ reactivity (approximately 2.5 min average lifetime) in canister samples collected during daytime showed a much larger loss rate for $NO_3$ to VOCs present in less aged air measured during daylight hours, indicating considerable potential for $NO_3$ oxidation chemistry within plumes closer to large emission sources at night. Finally, observations of small daytime $N_2O_5$ mixing ratios were consistent with its predicted photochemical steady state in an average sense. Observations during daytime polluted fog suggested a large discrepancy between observed and calculated $N_2O_5$ and an important role for heterogeneous uptake of $N_2O_5$ in cloud as a source of soluble nitrate during daytime.

**Acknowledgments**

S.S.B., W.P.D., and D.D.P. acknowledge support from the NOAA Atmospheric Chemistry, Climate and Carbon Cycle (AC4) program for this work. The Hong Kong team acknowledges support from the Hong Kong Research Grants Council (PolyU 153026/14P), the Hong Kong Environmental Protection Department, and the Hong Kong Polytechnic University. The authors would like to thank Xu Zheng and Wang Xinfeng for their support in setting up the site and to Peter K.K. Louie' and Connie W.Y. Luk for their help with access to the TMS site and for providing some TMS local wind data. Data are available upon request (steven.s.brown@noaa.gov, tao.wang@polyu.edu.hk).

## References

Atkinson, R., A. M. Winer, and J. N. Pitts Jr. (1986), Estimation of night-time $N_2O_5$ concentrations from ambient $NO_2$ and $NO_3$ radical concentrations and the role of $N_2O_5$ in night-time chemistry, *Atmos. Environ. 20*(2), 331–339.

Benton, A. K., J. M. Langridge, S. M. Ball, W. J. Bloss, M. Dall'Osto, E. Nemitz, R. M. Harrison, and R. L. Jones (2010), Night-time chemistry above London: Measurements of $NO_3$ and $N_2O_5$ from the BT Tower, *Atmos. Chem. Phys. 10*(20), 9781–9795, doi:10.5194/acp-10-9781-2010.

Bertram, T. H., and J. A. Thornton (2009), Toward a general parameterization of $N_2O_5$ reactivity on aqueous particles: The competing effects of particle liquid water, nitrate and chloride, *Atmos. Chem. Phys. 9*, 8351–8363.

Brown, S. S., and J. Stutz (2012), Nighttime radical observations and chemistry, *Chem. Soc. Rev. 41*, 6405–6447, doi:10.1039/c2cs35181a.

Brown, S. S., H. Stark, and A. R. Ravishankara (2003a), Applicability of the steady-state approximation to the interpretation of atmospheric observations of $NO_3$ and $N_2O_5$, *J. Geophys. Res.*, *108*(D17), 4539, doi:10.1029/2003JD003407.

Brown, S. S., H. Stark, T. B. Ryerson, E. J. Williams, D. K. J. Nicks, M. Trainer, F. C. Fehsenfeld, and A. R. Ravishankara (2003b), Nitrogen oxides in the nocturnal boundary layer: Simultaneous, in-situ detection of $NO_3$, $N_2O_5$, NO, $NO_2$ and $O_3$, *J. Geophys. Res.*, *108*(D9), 4299, doi:10.1029/2002JD002917.

Brown, S. S., et al. (2004), Nighttime removal of $NO_x$ in the summer marine boundary layer, *Geophys. Res. Lett.*, *31*, L07108, doi:10.1029/2004GL019412.

Brown, S. S., et al. (2005), Aircraft observations of daytime $NO_3$ and $N_2O_5$ and their implications for tropospheric chemistry, *J. Photochem. Photobiol. A*, *176*(1–3), 270–278.

Brown, S. S., et al. (2006a), Nocturnal odd-oxygen budget and its implications for ozone loss in the lower troposphere, *Geophys. Res. Lett.*, *33*, L08801, doi:10.1029/2006GL025900.

Brown, S. S., et al. (2006b), Variability in nocturnal nitrogen oxide processing and its role in regional air quality, *Science*, *311*, 67–70.

Brown, S. S., et al. (2007), Vertical profiles in $NO_3$ and $N_2O_5$ measured from an aircraft: Results from the NOAA P-3 and surface platforms during NEAQS 2004, *J. Geophys. Res.*, *112*, D22304, doi:10.1029/2007JD008883.

Brown, S. S., et al. (2009), Reactive uptake coefficients for $N_2O_5$ determined from aircraft measurements during TexAQS 2006: Comparison to current model parameterizations, *J. Geophys. Res.*, *114*, D00F10, doi:10.1029/2008JD011679.

Brown, S. S., et al. (2011), Budgets for nocturnal VOC oxidation by nitrate radicals aloft during the 2006 Texas Air Quality Study, *J. Geophys. Res.*, *116*, D24305, doi:10.1029/2011JD016544.

Cooper, O. R., R.-S. Gao, D. Tarasick, T. Leblanc, and C. Sweeney (2012), Long-term ozone trends at rural ozone monitoring sites across the United States, 1990–2010, *J. Geophys. Res.*, *117*, D22307, doi:10.1029/2012JD018261.

Crowley, J. N., G. Schuster, N. Pouvesle, U. Parchatka, H. Fischer, B. Bonn, H. Bingemer, and J. Lelieveld (2010), Nocturnal nitrogen oxides at a rural mountain-site in south-western Germany, *Atmos. Chem. Phys. 10*(6), 2795–2812.

Day, D. A., M. B. Dillon, P. J. Wooldridge, J. A. Thornton, R. S. Rosen, E. C. Wood, and R. C. Cohen (2003), On alkyl nitrates, $O_3$, and the "missing $NO_y$", *J. Geophys. Res.*, *108*(D16), 4501, doi:10.1029/2003JD003685.

Draxler, R. R., and G. D. Rolph (2003), HYSPLIT (HYbrid Single-Particle Lagrangian Integrated Tracker) Model access via NOAA ARL Ready Website [Available at http://www.arl.noaa.gov/ready/hysplit4.html, NOAA Air Resources Laboratory, Silver Spring, MD].

Fuchs, H., W. P. Dubé, S. J. Ciciora, and S. S. Brown (2008), Determination of inlet transmission and conversion efficiencies for in situ measurements of the nocturnal nitrogen oxides, $NO_3$, $N_2O_5$ and $NO_2$, via pulsed cavity ring-down spectroscopy, *Anal. Chem. 80*(15), 6010–6017, doi:10.1021/ac8007253.

Geyer, A., et al. (2003), Direct observations of daytime $NO_3$: Implications for urban boundary layer chemistry, *J. Geophys. Res.*, *108*(D12), 4368, doi:10.1029/2002JD002967.

Guo, S., et al. (2014), Elucidating severe urban haze formation in China, *Proc. Natl. Acad. Sci. U. S. A. 111*(49), 17,373–17,378.

Hilboll, A., A. Richter, and J. P. Burrows (2013), Long-term changes of tropospheric $NO_2$ over megacities derived from multiple satellite instruments, *Atmos. Chem. Phys. 13*(8), 4145–4169, doi:10.5194/acp-13-4145-2013.

Huang, R.-J., et al. (2014), High secondary aerosol contribution to particulate pollution during haze events in China, *Nature*, advance online publication, doi:10.1038/nature13774.

Kennedy, O. J., et al. (2011), An aircraft based three channel broadband cavity enhanced absorption spectrometer for simultaneous measurements of $NO_3$, $N_2O_5$ and $NO_2$, *Atmos. Meas. Tech. 4*, 1759–1776, doi:10.5194/amtd-4-3499-2011.

Lelieveld, J., and P. J. Crutzen (1990), Influences of cloud photochemical processes on tropospheric ozone, *Nature*, *343*, 227–233.

Osthoff, H. D., et al. (2006), Observations of daytime $N_2O_5$ in the marine boundary layer during New England Air Quality Study—Intercontinental Transport and Chemical Transformation 2004, *J. Geophys. Res.*, *111*, D23S14, doi:10.1029/2006JD007593.

Osthoff, H. D., M. J. Pilling, A. R. Ravishankara, and S. S. Brown (2007), Temperature dependence of the $NO_3$ absorption cross section above 298 K and determination of the equilibrium constant for $NO_3 + NO_2 <--> N_2O_5$ at atmospherically relevant conditions, *Phys. Chem. Chem. Phys. 9*, 5785–5793, doi:10.1039/b709193a.

Parrish, D. D., et al. (2008), Overview of the Second Texas Air Quality Study (TexAQS II) and the Gulf of Mexico Atmospheric Composition and Climate Study (GoMACCS), *J. Geophys. Res.*, *114*, D00F13, doi:10.1029/2009JD011842.

Pathak, R. K., W. S. Wu, and T. Wang (2009), Summertime $PM_{2.5}$ ionic species in four major cities of China: Nitrate formation in an ammonia-deficient atmosphere, *Atmos. Chem. Phys. 9*, 1711–1722.

Pathak, R. K., T. Wang, and W. S. Wu (2011), Nighttime enhancement of $PM_{2.5}$ nitrate in ammonia-poor atmospheric conditions in Beijing and Shanghai: Plausible contributions of heterogeneous hydrolysis of $N_2O_5$ and $HNO_3$ partitioning, *Atmos. Environ. 45*(5), 1183–1191.

Platt, U., G. LeBras, G. Poulet, J. P. Burrows, and G. Moortgat (1990), Peroxy radicals from night-time reactions of $NO_3$ with organic compounds, *Nature*, *348*, 147–149.

Platt, U. F., A. M. Winer, H. W. Bierman, R. Atkinson, and J. N. Pitts Jr. (1984), Measurement of nitrate radical concentrations in continental air, *Environ. Sci. Technol. 18*, 365–369.

Pye, H. O. T., A. W. H. Chan, M. P. Barkley, and J. H. Seinfeld (2010), Global modeling of organic aerosol: The importance of reactive nitrogen ($NO_x$ and $NO_3$), *Atmos. Chem. Phys. 10*(22), 11,261–11,276, doi:10.5194/acp-10-11261-2010.

Roberts, J. M., H. D. Osthoff, S. S. Brown, and A. R. Ravishankara (2009), Laboratory studies of products of $N_2O_5$ uptake on $Cl^-$ containing substrates, *Geophys. Res. Lett.*, *36*, L20808, doi:10.1029/2009GL040448.

Russell, A. R., L. C. Valin, and R. C. Cohen (2012), Trends in OMI $NO_2$ observations over the United States: Effects of emission control technology and the economic recession, *Atmos. Chem. Phys. 12*(24), 12,197–12,209, doi:10.5194/acp-12-12197-2012.

Sander, S. P., et al. (2011), *Chemical Kinetics and Photochemical Data for Use in Atmospheric Studies*, JPL Publication 10–6, Pasadena, Calif.

Simon, H., A. Reff, B. Wells, J. Xing, and N. Frank (2014), Ozone trends across the United States over a period of decreasing $NO_x$ and VOC emissions, *Environ. Sci. Technol. 49*(1), 186–195, doi:10.1021/es504514z.

Stull, R. B. (1988), *An Introduction to Boundary Layer Meteorology*, Kluwer Academic, Dordrecht, Netherlands.

Stutz, J., B. Alicke, R. Ackermann, A. Geyer, A. B. White, and E. Williams (2004), Vertical profiles of $NO_3$, $N_2O_5$, $O_3$, and $NO_x$ in the nocturnal boundary layer: 1. Observations during the Texas Air Quality Study 2000, *J. Geophys. Res.*, *109*, D12306, doi:10.1029/2003JD004209.

Tang, G., X. Li, Y. Wang, J. Xin, and X. Ren (2009), Surface ozone trend details and interpretations in Beijing, 2001–2006, *Atmos. Chem. Phys. 9*(22), 8813–8823.

Thornton, J. A., et al. (2010), A large atomic chlorine source inferred from mid-continental reactive nitrogen chemistry, *Nature*, *464*, 271–274.

Wagner, N. L., W. P. Dubé, R. A. Washenfelder, C. J. Young, I. B. Pollack, T. B. Ryerson, and S. S. Brown (2011), Diode laser-based cavity ring-down instrument for $NO_3$, $N_2O_5$, NO, $NO_2$ and $O_3$ from aircraft, *Atmos. Meas. Tech. 4*, 1227–1240.

Wagner, N. L., et al. (2013), $N_2O_5$ uptake coefficients and nocturnal $NO_2$ removal rates determined from ambient wintertime measurements, *J. Geophys. Res. Atmos. 118*, 9331–9350, doi:10.1002/jgrd.50653.

Wang, S., C. Shi, B. Zhou, H. Zhao, Z. Wang, S. Yang, and L. Chen (2013), Observation of $NO_3$ radicals over Shanghai, China, *Atmos. Environ. 70*, 401–409, doi:10.1016/j.atmosenv.2013.01.022.

Wang, T., A. Ding, J. Gao, and W. S. Wu (2006), Strong ozone production in urban plumes from Beijing, China, *Geophys. Res. Lett.*, *33*, L21806, doi:10.1029/22006GL027689.

Wang, T., X. L. Wei, A. J. Ding, C. N. Poon, K. S. Lam, Y. S. Li, L. Y. Chan, and M. Anson (2009), Increasing surface ozone concentrations in the background atmosphere of Southern China, 1994–2007, *Atmos. Chem. Phys. 9*(16), 6217–6227.

Wang, T., et al. (2016), Observations of nitryl chloride and modeling its source and effect on ozone in the planetary boundary layer of southern China, *J. Geophys. Res. Atmos.*, *121*, doi:10.1002/2015JD024556.

Wang, X., T. Wang, C. Yan, Y. J. Tham, L. Xue, Z. Xu, and Q. Zha (2014), Large daytime signals of $N_2O_5$ and NO3 inferred at 62 amu in a TD-CIMS: Chemical interference or a real atmospheric phenomenon? *Atmos. Meas. Tech. 7*(1), 1–12, doi:10.5194/amt-7-1-2014.

Winer, A. M., R. Atkinson, and J. N. J. Pitts (1984), Gaseous nitrate radical: Possible nighttime atmospheric sink for biogenic organic compounds, *Science*, *224*, 156–158.

Xue, J., Z. Yuan, A. K. H. Lau, and J. Z. Yu (2014), Insights into factors affecting nitrate in $PM_{2.5}$ in a polluted high $NO_x$ environment through hourly observations and size distribution measurements, *J. Geophys. Res. Atmos. 119*, 4888–4902, doi:10.1002/2013JD021108.

Yang, D., C. Li, A. K. H. Lau, and Y. Li (2013), Long-term measurement of daytime atmospheric mixing layer height over Hong Kong, *J. Geophys. Res. Atmos. 118*, 2422–2433, doi:10.1002/jgrd.50251.

Zheng, B., Q. Zhang, Y. Zhang, K. B. He, K. Wang, G. J. Zheng, F. K. Duan, Y. L. Ma, and T. Kimoto (2015), Heterogeneous chemistry: a mechanism missing in current models to explain secondary inorganic aerosol formation during the January 2013 haze episode in North China, *Atmos. Chem. Phys. 15*(4), 2031–2049, doi:10.5194/acp-15-2031-2015.